A model-free Data-Driven paradigm for *in situ* patient-specific prediction of human brain response to ultrasound stimulation

Hossein Salahshoor[1], Michael Ortiz[1,*]

1 Division of Engineering and Applied Science, California Institute of Technology, 1200 E California Blvd, Pasadena, CA 91125

*** ortiz@caltech.edu**

Abstract

We present a class of model-free Data-Driven solvers that effectively enable the utilization of *in situ* and *in vivo* imaging data *directly* in full-scale calculations of the mechanical response of the human brain to ultrasound stimulation, entirely bypassing the need for analytical modeling or regression of the data. We demonstrate the approach, including its ability to make detailed spatially-resolved patient-specific predictions of wave patterns, using public-domain MRI images, MRE data and commercially available solid-mechanics software.

Significance statement

Accurate patient-specific computational models of wave propagation in the human brain are fundamental for understanding the complex wave patterns induced by ultrasound (US) stimulation with a view to improving and optimizing clinical procedures. A critical bottleneck in the predictive ability of computational models has been the complexity, paucity of data and observational uncertainty pertaining to the mechanical behavior of brain tissue, both healthy and diseased. Recent developments of advanced microscopy methods, such as Magnetic Resonance Elastography (MRE) enable the *in situ* and *in vivo* characterization of the viscoelastic response of the brain tissue of individual patients in a clinical environment. We develop a new model-free Data-Driven framework that directly incorporates patient-specific data on-the-fly into calculations of wave patterns in the brain resulting from US stimulation. We demonstrate the framework by performing full-scale spatially-resolved calculations based on public domain viscoelastic data from MRE measurements.

Introduction

Predictive modeling of the mechanical response of the human brain to ultrasound stimulation is an important part of many preventive, diagnostic, and therapeutic biomedical procedures [2,14,18,19]. Computational models are increasingly incorporated to inform or guide biomedical research such as transcranial ultrasound stimulation therapies. However, the efficacy of such models depends crucially on precise patient-specific representations of both the geometry and the material response of the brain *in vivo* [5,13,21].

In contrast to recent advances in high-resolution, patient-specific, *in-vivo*, and non-invasive imaging techniques, which presently enable accurate representations of

brain anatomy down to ultra-fine features [7,8], the accurate and reliable material modeling of brain tissue has proven challenging and remains a major predictive bottleneck [3,4]. These modeling challenges arise from the ultra-compliant, complex, heterogeneous, and patient-specific nature of the mechanical properties of brain tissue [3]. These complexities cannot easily be reduced to analytical formulas that differentiate, e.g., between healthy and diseased tissue and the presence of tumors and other lesions in a particular patient.

By way of contrast, recent advances in microscopy and elastography techniques, such as Magnetic Resonance Elastography (MRE) [12], have made possible the *in vivo* characterization of the viscoelastic response of brain tissue in individual patients. Indeed, MRE technology presently allows personalized atlases of brain-tissue viscoelastic properties, including storage and loss moduli as functions of frequency, to be compiled *in vivo* [1,9]. These advances have radically transformed brain biomechanics from a data-starved to a data-rich field, a transformation that challenges theory and computational practice in fundamental and far-reaching ways.

Several possible strategies can be pursued in response to these challenges and opportunities. One currently popular strategy uses Machine Learning (ML) regression in order to fit the data, e.g., using neural-network representations [22]. However, any method of regression, whether based on neural networks or on some other functional representation, is necessarily *lossy*. Indeed, regression replaces the empirical data set by a fitted function, a process that inevitably results in loss of information, biases and uncontrolled modeling errors. In addition, models need to be trained *in situ* for specific patients, which is costly and time consuming.

An appealing alternative is to formulate solvers that effectively enable the utilization of *in situ* and *in vivo* imaging data *directly* in calculations, thus entirely bypassing the intermediate material modeling step. In this work, we demonstrate how one such model-free Data-Driven paradigm [17] can be used to forge a direct connection between *in situ* and *in vivo* patient-specific measurements of viscoelastic brain-tissue properties and real-time full-scale calculations of the mechanical response of the human brain to ultrasound stimulation, cf. Section 1. For purposes of demonstration and verification, we specifically use a public-domain MRE data set [9] and the corresponding MNI stereotaxic space to develop a finite-element model of the human brain co-registered with the voxel-based MRE data. We then use our model-free Data-Driven solver [17] to compute, directly from the data, wave patterns in the brain resulting from transcranial ultrasound stimulation, cf. Section 2.

The model-free Data-Driven approach demonstrated in this paper suggests a natural path for achieving on-the-fly patient-specific predictions of brain mechanics in a clinical environment. We illustrate the patient-specific aspect of our model-free Data-Driven brain approach by considering MRE data sets from eight different healthy human subjects from the repository provided by [9]. The computed shear strain amplitudes exhibit variations of up to 25%, which, as expected, bears out the need for patient-specific predictions.

We anticipate that strictly Data-Driven approaches such as demonstrated here will supply a valuable basis for developing and optimizing patient-specific therapeutic procedures in the future.

1 Data-Driven brain mechanics

A schematic of the proposed model-free Data-Driven framework is shown in Fig. 1. We use anatomical data, in the form of MRI images, Fig. 1 top-left, in conjunction with a co-registered atlas of viscoleastic properties of the brain tissue, Fig. 1 bottom-left, to generate a finite-element model of the brain, Fig. 1 top-right. We choose the

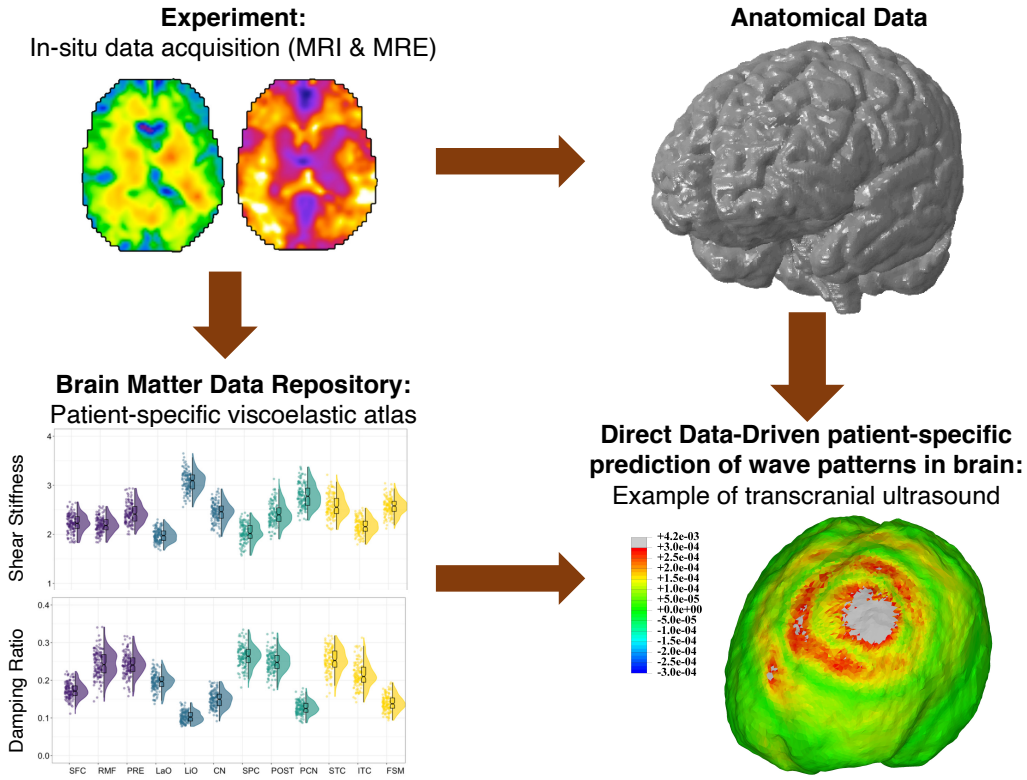

Figure 1. Schematic of the model-free Data-Driven brain mechanics paradigm. Top-left: anatomical data in the form of MRI images. Bottom-left: co-registered atlas of viscoleastic properties of the brain tissue. Top-right: finite-element model of the brain. Bottom-right: steady-state wave pattern induced by low-intensity focus ultrasound (LIFUS) applied to a region on the frontal lobe.

finite-element mesh size equal to, or smaller than, the voxel size in the MRE atlas, so that every material point in the mesh can be assigned to a unique MRE voxel. The bone tissue is assumed to be linear elastic. We then solve in the frequency domain for the steady-state wave pattern induced by low-intensity focus ultrasound (LIFUS) applied to a region on the frontal lobe, Fig. 1 bottom-right. Specifically, the Data-Driven solver endeavors to minimize the discrepancy between local material states in the finite-element model and the MRE data while simultaneously enforcing dynamic equilibrium in the sense of the Helmholtz equation. Conveniently, the solver can be implemented as a wrapper around conventional FE element programs, including commercially available software. A complete mathematical description of the Data-Driven solver and an assessment of convergence with respect to the data may be found [17].

2 Predicting wave patterns in transcranial ultrasound stimulation

We demonstrate the range and scope of the model-free Data-Driven brain mechanics framework through an application to transcranial ultrasound stimulation. Transcranial ultrasound has elicited growing interest in both low-intensity mode, suited to neuromodulation applications [2,10,14–16,18–20], as well as in high-intensity mode,

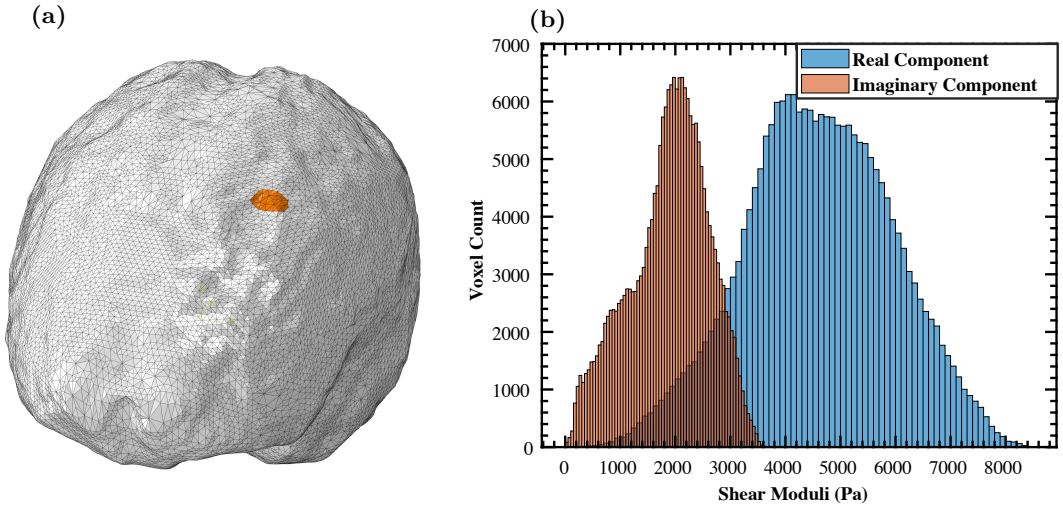

Figure 2. (A): Finite element model of a heterogeneous brain with 0.2 million tetrahedral elements. Transcranial ultrasound stimulation is modeled by subjecting the highlighted region to ultrasound pressure as a traction boundary condition. (B): histogram of complex shear moduli from MRE data. The computational model is co-registered to the data. Both the geometry and viscoelastic map are obtained from public domain MRE data [9].

germane to tumor ablation applications [11, 23].

For purposes of demonstration, we use the recently published atlas of viscoelastic properties of brain tissue [9], acquired at a single frequency of 50 Hz from 134 human subjects. We also adopt the associated MNI coordinate data to develop a computational heterogeneous brain model, co-registered to the MRE data. The resultant geometry is discretized into a finite element model comprising 0.2 million three-dimensional tetrahedral elements, Fig. 2a. We note that the MRE data encodes complex viscoelastic shear moduli with real and imaginary components, corresponding to storage and loss moduli for each material point, respectively. For the sake of simplicity, we assume the brain matter to be isotropic, with an elastic bulk modulus of 2 GPa assigned to the entire model. We remark that, conditioned on the availability of the data, the present framework can account for fully anisotropic brain matter or other material symmetries thereof. Fig. 2b shows a histogram of the complex moduli in the material data set binned by voxel. The wide spread of properties in the material data set resulting from material heterogeneity, patient-to-patient variability and measurement scatter is noteworthy.

We subject a small region on the frontal lobe of the brain, shown in orange in Fig. 2, to a sinusoidal pressure with a peak amplitude of 60 kPa. Calculations were performed using the commercial finite-element software Abaqus (Abaqus/Standard, Dassault Systemes Simulia, France) as compute engine within the model-free Data-Driven wrapper. Fig. 3 shows computed contours of the real and imaginary components of all six components of the strain tensor across the entire brain. The relatively higher magnitude of the shear strains with respect to volumetric strains is expected from the softness of the brain tissue in shear. The relative ease of implementation of the framework on top of readily available commercial software and the speed of the calculations, comparable to that of a simple elastic analysis, are also noteworthy.

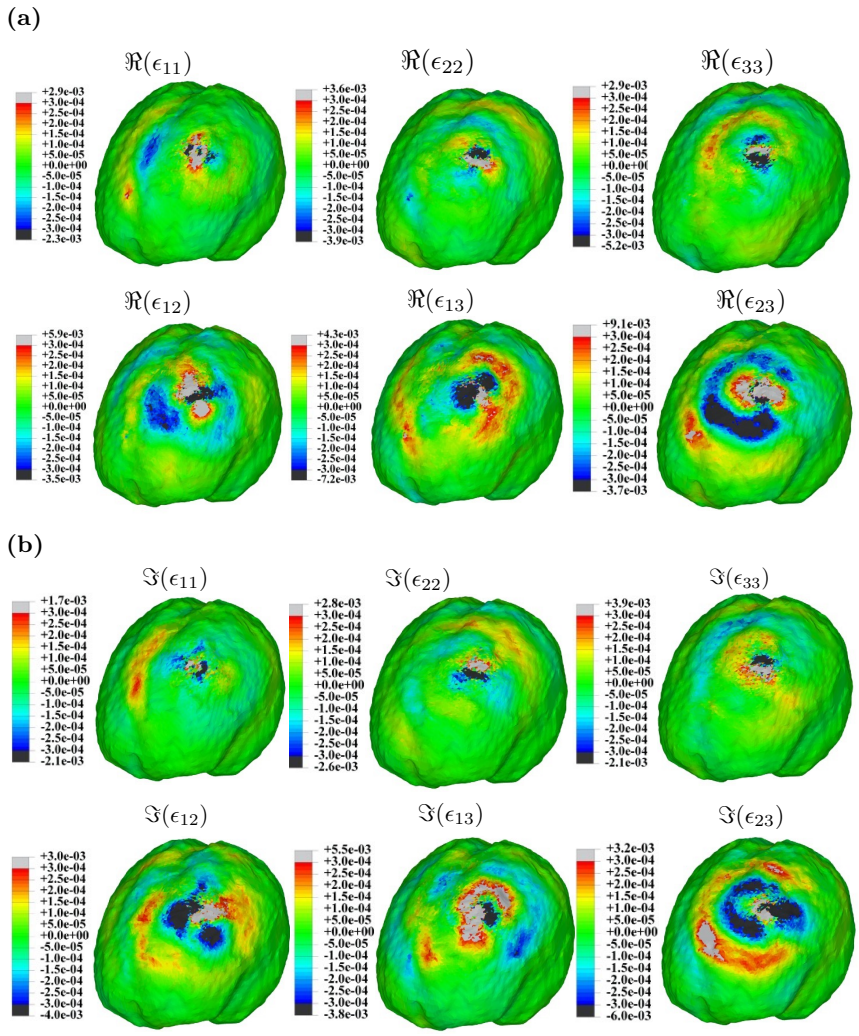

Figure 3. Model-free Data-Driven simulation of transcranial ultrasound stimulation on a region on the frontal lobe of brain, Fig. 2a. Spatial distribution of components of strain at steady state. a) Real part; b) Imaginary part.

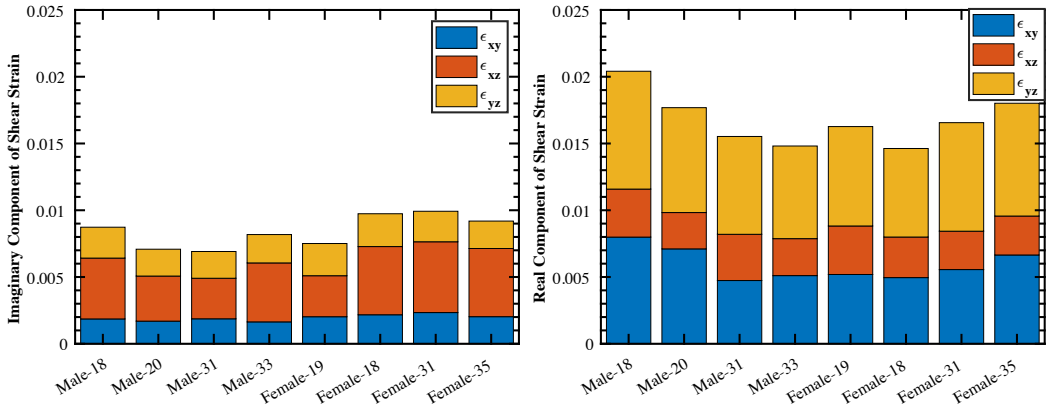

Figure 4. Model-free Data-Driven simulation of transcranial ultrasound stimulation on a region on the frontal lobe of brain, Fig. 2a, for eight patient-specific MRE data sets. Maximum strain amplitudes at steady state. Left: Imaginary part; Right: Real part.

3 Patient-specific modeling

We illustrate the patient-specific aspect of our model-free Data-Driven brain approach by considering MRE data sets from eight different healthy human subjects from the repository provided by [9]. The subjects were four male and four female with ages varying from 18 to 35. As in the preceding section, we solve the corresponding eight Data-Driven problems of transcranial ultrasound stimulation with all components of the computational model held fixed except for the complex moduli data. Histograms of the material data set binned by voxel for all eight patients are depicted in the supplementary file. We again emphasize that all calculations are based directly on the MRE data without recourse to analytical modeling of the data at any stage of the calculations.

Fig. 4 shows the computed maximum complex amplitude of harmonic shear strains at a frequency of 50 Hz for all eight patients. The appendix contains the computed contours of real and imaginary components of both maximum and minimum principal strain across the entire brain for all eight patients. We observe that the real component of maximum shear strain ϵ_{xy} varies from 0.015 to 0.021, or a 25% spread, with similar variations for the remaining components. As expected, these results bear out the importance of patient-specific data and illustrate the potential of model-free Data-Driven methods for achieving patient specificity on demand in a clinical environment.

Materials and Methods

A detailed summary of the method in presented in the SI Appendix. The model-free Data-Driven solver strives to find admissible states of stress and strain in the finite-element model that are closest to the material data set in the sense of a suitable measure of discrepancy [17]. The finite-element model supplies a representation of the geometry of the brain, which is assumed to be free-standing, and the ultrasound pressure loading applied to it. It also provides a means of enforcing admissibility of the fields, i. e., strain compatibility and stress equilibrium. The material behavior of the brain tissue is assumed to be linear viscoelastic. The problem of wave propagation is formulated in the frequency domain and is governed by the complex Helmholtz equation.

The viscoelastic behavior of the brain tissue is characterized by empirical data sampling the dependence of the complex modulus on frequency. The data may be noisy owing to measurement error and experimental scatter. The discrepancy between finite-element stress and strain field and the material data is minimized iteratively. The requisite finite-element calculations are conducted using the commercial code Abaqus (Abaqus/Standard, Dassault Systemes Simulia, France). A detailed analysis of the well-posedness of the method and convergence with respect to data is presented in [6] for the elastic case.

Data availability

The data that support the findings of this study are available within this article and references therein. The simulation protocols are also available from the corresponding author upon request.

Acknowlegments

This project was supported by U.S. National Institutes of Health Grant No. 1RF1MH117080.

References

1. P. V. Bayly, A. Alshareef, A. K. Knutsen, K. Upadhyay, R. J. Okamoto, A. Carass, J. A. Butman, D. L. Pham, J. L. Prince, K. Ramesh, et al. Mr imaging of human brain mechanics in vivo: new measurements to facilitate the development of computational models of brain injury. *Annals of biomedical engineering*, 49(10):2677–2692, 2021.

2. J. Blackmore, S. Shrivastava, J. Sallet, C. R. Butler, and R. O. Cleveland. Ultrasound neuromodulation: a review of results, mechanisms and safety. *Ultrasound in medicine & biology*, 45(7):1509–1536, 2019.

3. S. Budday, T. C. Ovaert, G. A. Holzapfel, P. Steinmann, and E. Kuhl. Fifty shades of brain: a review on the mechanical testing and modeling of brain tissue. *Archives of Computational Methods in Engineering*, 27(4):1187–1230, 2020.

4. S. Chatelin, A. Constantinesco, and R. Willinger. Fifty years of brain tissue mechanical testing: from in vitro to in vivo investigations. *Biorheology*, 47(5-6):255–276, 2010.

5. A. Chaturvedi, C. R. Butson, S. F. Lempka, S. E. Cooper, and C. C. McIntyre. Patient-specific models of deep brain stimulation: influence of field model complexity on neural activation predictions. *Brain stimulation*, 3(2):65–77, 2010.

6. S. Conti, S. Müller, and M. Ortiz. Data-driven problems in elasticity. *Archive for Rational Mechanics and Analysis*, 229:79–123, 2018.

7. A. M. Dale, A. K. Liu, B. R. Fischl, R. L. Buckner, J. W. Belliveau, J. D. Lewine, and E. Halgren. Dynamic statistical parametric mapping: combining fmri and meg for high-resolution imaging of cortical activity. *neuron*, 26(1):55–67, 2000.

8. C. Errico, J. Pierre, S. Pezet, Y. Desailly, Z. Lenkei, O. Couture, and M. Tanter. Ultrafast ultrasound localization microscopy for deep super-resolution vascular imaging. *Nature*, 527(7579):499–502, 2015.

9. L. V. Hiscox, M. D. McGarry, H. Schwarb, E. E. Van Houten, R. T. Pohlig, N. Roberts, G. R. Huesmann, A. Z. Burzynska, B. P. Sutton, C. H. Hillman, et al. Standard-space atlas of the viscoelastic properties of the human brain. *Human brain mapping*, 41(18):5282–5300, 2020.

10. A. Jerusalem, Z. Al-Rekabi, H. Chen, A. Ercole, M. Malboubi, M. Tamayo-Elizalde, L. Verhagen, and S. Contera. Electrophysiological-mechanical coupling in the neuronal membrane and its role in ultrasound neuromodulation and general anaesthesia. *Acta biomaterialia*, 2019.

11. G. Mauri, L. Nicosia, Z. Xu, S. Di Pietro, L. Monfardini, G. Bonomo, G. M. Varano, F. Prada, P. Della Vigna, and F. Orsi. Focused ultrasound: tumour ablation and its potential to enhance immunological therapy to cancer. *The British journal of radiology*, 91(xxxx):20170641, 2018.

12. R. Muthupillai, D. Lomas, P. Rossman, J. F. Greenleaf, A. Manduca, and R. L. Ehman. Magnetic resonance elastography by direct visualization of propagating acoustic strain waves. *science*, 269(5232):1854–1857, 1995.

13. M. L. Neal and R. Kerckhoffs. Current progress in patient-specific modeling. *Briefings in bioinformatics*, 11(1):111–126, 2010.

14. C. Rabut, S. Yoo, R. C. Hurt, Z. Jin, H. Li, H. Guo, B. Ling, and M. G. Shapiro. Ultrasound technologies for imaging and modulating neural activity. *Neuron*, 108(1):93–110, 2020.

15. J. L. Robertson, B. T. Cox, J. Jaros, and B. E. Treeby. Accurate simulation of transcranial ultrasound propagation for ultrasonic neuromodulation and stimulation. *The Journal of the Acoustical Society of America*, 141(3):1726–1738, 2017.

16. H. Salahshoor, H. Guo, M. G. Shapiro, and M. Ortiz. Mechanics of ultrasonic neuromodulation in a mouse subject. *Extreme Mechanics Letters*, 50:101539, 2022.

17. H. Salahshoor and M. Ortiz. Model-free data-driven viscoelasticity in the frequency domain. *arXiv preprint arXiv:2205.06674*, 2022.

18. H. Salahshoor, M. G. Shapiro, and M. Ortiz. Transcranial focused ultrasound generates skull-conducted shear waves: Computational model and implications for neuromodulation. *Applied Physics Letters*, 117(3):033702, 2020.

19. T. Sato, M. G. Shapiro, and D. Y. Tsao. Ultrasonic neuromodulation causes widespread cortical activation via an indirect auditory mechanism. *Neuron*, 98(5):1031–1041, 2018.

20. W. J. Tyler. Noninvasive neuromodulation with ultrasound? a continuum mechanics hypothesis. *The Neuroscientist*, 17(1):25–36, 2011.

21. A. Wittek, K. Miller, R. Kikinis, and S. K. Warfield. Patient-specific model of brain deformation: Application to medical image registration. *Journal of biomechanics*, 40(4):919–929, 2007.

22. K. Xu, A. M. Tartakovsky, J. Burghardt, and E. Darve. Learning viscoelasticity models from indirect data using deep neural networks. *Computer Methods in Applied Mechanics and Engineering*, 387:114124, 2021.

23. Y.-F. Zhou. High intensity focused ultrasound in clinical tumor ablation. *World journal of clinical oncology*, 2(1):8, 2011.

Supporting Information Text

Data-driven viscoelasticity in the frequency domain

Let us consider a discretized model of brain comprised of N nodes and M voxels, or material points. The discrete form of the governing equations of elastodynamics in the frequency domain are of the general form:

$$\hat{\epsilon_e}(\omega) = B_e \hat{u}(\omega), e = 1, ..., M \quad [1a]$$

$$B_e^T w_e \hat{\sigma_e}(\omega) - M_e \omega^2 \hat{u}(\omega) = \hat{f}_e(\omega), \quad [1b]$$

where σ_e and ϵ_e are the local stress and strain vectors, B_e is the strain-displacement matrix, M_e is the mass matrix, and w is the weight corresponding to the element volume. Note that $\hat{}$ denotes the Fourier transform and ω is the frequency. The mechanical state of brain is characterized by a global phase space $Z = Z_1 \times Z_2 \times ... \times Z_M$, where each local phase space Z_e is comprised of local pairs of stress and strain $z_e = \{(\hat{\epsilon}_e, \hat{\sigma}_e)\}_{e=1}^M$. Since the MRE experiments and the corresponding data are harmonic states, and given the fact that harmonic functions are represented by Dirac measures in Fourier space, we restrict our attention to strains and stresses that are represented by Dirac measures centered at the frequency ω.

The viscoelastic response of the tissue can be represented by the Boltzmann superposition principle:

$$\sigma(t) = \int_{-\infty}^{t} \mathbb{J}(t-\tau)\epsilon(\tau)d\tau. \quad [2]$$

Using the convolution theorem, the Fourier transform of Eq. (2) is obtained as:

$$\hat{\sigma}(\omega) = \mathbb{E}(\omega)\hat{\epsilon}(\omega). \quad [3]$$

The complex modulus $\mathbb{E}$ is comprised of a real part, or the storage modulus, and an imaginary part, referred to as loss modulus. In the classical approach, the MRE data is incorporated to fit a viscoelastic model to obtain the function $\mathbb{E}(\omega)$.

An indispensable problem with the classical approach just described is that, whereas the field equations Eq. (1) are known exactly and are uncertainty-free, the material law Eq. (3) is known only empirically through experimental data. These data are fit to models that essentially lack a fundamental and physical basis, and are often designed to achieve particular goals. Moreover, it is often observed that the viscoelastic models are not able to capture the response of the material outside the range of the data that was initially utilized for the fit, which often serves as the underlying motivation for developing new models, such as fractional viscoleascitiy. The situation is only exasperated throughout the fitting process, when a functional form is fixed and the corresponding parameters are sought. This is due to the fact that the choice of parameters like relaxation times are ambiguous.

We develop a drastically different approach here, where the predictions are made directly from the field equations and experimental data. Let us define a subspace, or constraint set, in the global phase space Z:

$$\mathcal{E} = \{z \in Z : \text{Eq. (1a) and Eq. (1b)}\}, \quad [4]$$

amounting to the set all the states satisfying compatibility and equilibrium at each material . Let us denote the MRE data set as $\mathcal{U} = \{(\omega^i, \mathbb{E}_e^i), i = 1, ..., V, e = 1, ..., M\}$, where V and M are the total number of MRE excitation frequencies and voxels, respectively. We then define all the states that are obtained from the MRE data set as:

$$\mathcal{D} = \prod_{i=1}^{V}\prod_{e=1}^{M} \mathcal{D}_e^i = \prod_{i=1}^{V}\prod_{e=1}^{M} \{z_e \in Z_e : \hat{\sigma}_e = \mathbb{E}_e^i \hat{\epsilon}_e \text{ where } \mathbb{E}_e^i \in \mathcal{U}\}. \quad [5]$$

The MRE data-driven brain mechanics problem is then defined as finding the equilibrated and compatible state at each brain voxel that minimizes the distance to the data set $\mathcal{D}$. To this end, we need a notion of metric in phase space Z. Recalling that the phase space is comprised of Dirac measures, we need a notion of metric that incorporates the distance between both the frequencies and the amplitudes. With recourse to the optimal transport theory, we incorporate the notion of *flat norm* $||.||_F$. Apart from being natural, the flat norm distance affords the great practical advantage of enabling the use of data at frequencies other that the applied frequencies of excitation, with an appropriate penalty accorded to the discrepancy between the two. This property is specially advantageous with the MRE experiments, where the data are sampled at discrete frequencies, which are likely to differ from the frequency that will be utilized in subsequent modelings.

For present purposes, and for the sake of completeness, it only need to characterize the flat-norm distance between harmonic histories. For a precise definition of flat norm and the proof of the following formulas, we refer the reader to [16]. Let us consider two states $\hat{z}_e' = Z_e' \delta_{\omega'}$ and $\hat{z}_e'' = Z_e'' \delta_{\omega''}$ as Dirac measures with complex amplitudes Z_e' and Z_e'' and frequencies ω' and ω''. The flat norm is computed as:

$$||Z_e' \delta_{\omega'} - Z_e'' \delta_{\omega''}||_F = \min\{||Z_e'||, ||Z_e''||\}\alpha + ||Z_e' - Z_e''||, \quad [6]$$

where $\alpha = \min\{2, |\omega' - \omega''|/\omega_c\}$, with ω_c representing a cutoff frequency. Furthermore, the distance $||.||$ is defined for each amplitude $Z_e = (E_e, S_e)$ as:

$$||Z_e||^2 = C||E_e||^2 + C^{-1}||S_e||^2, \quad [7]$$

where C is a parameter introduced to even out dimensions.

The MRE data are encoded as a set of complex moduli $\mathbb{E}$ and frequency ω, where each pair of $(\omega, \mathbb{E})$ parameterize a subspace in the phase space, which, in turn, translates in the data-driven problem thereof to be a distance minimization among the constraint set and a family of subspaces. We thus need to compute the flat norm distance between a Dirac measure and a subspace $\mathcal{L} = \{(Z_e = (E_e, S_e)|S_e = \mathbb{E}(\omega)E_e\}$ of the phase space:

$$d_F(Z_e\delta_\Omega, \mathcal{L}) = ||\tilde{Z}_e|| + \alpha\mu||Z_e^{||}||, \tag{8a}$$

$$\tilde{Z}_e = (\mu - 1)Z_e^{||} - Z_e^{\perp}, \tag{8b}$$

$$Z_e^{||} = \frac{1}{C^2 + \mathbb{E}^2}\begin{bmatrix} C^2E_e + \mathbb{E}S_e \\ \mathbb{E}(C^2E_e + \mathbb{E}S_e) \end{bmatrix}, \tag{8c}$$

$$Z_e^{\perp} = \frac{1}{C^2 + \mathbb{E}^2}\begin{bmatrix} \mathbb{E}(\mathbb{E}E_e - S_e) \\ C^2(S_e - \mathbb{E}E_e) \end{bmatrix}, \tag{8d}$$

$$\mu = 1 - \frac{\alpha}{\sqrt{1-\alpha^2}}\frac{||Z_e^{\perp}||}{||Z_e^{||}}, \tag{8e}$$

where all the norms are computed using Eq. (7).

With the foregoing notion of metric on the phase space, we then construct the data-driven problem as:

$$\inf_{y\in\mathcal{D}}\inf_{z\in\mathcal{E}}\sum_{e=1}^{M}||y_e - z_e||_F \tag{9}$$

A simple Data-Driven solver consists of the fixed point iteration [16]:

$$z_{j+1} = P_{\mathcal{E}}P_{\mathcal{D}}z_j, \tag{10}$$

for $j = 0, 1, ...$ and $z_0 \in Z$ arbitrary, where $P_{\mathcal{D}}$ and $P_{\mathcal{E}}$ denotes the closest point projection in Z onto $\mathcal{D}$ and $\mathcal{E}$. This solver Eq. (10) first projects z_j to the material data set $\mathcal{D}$ through the projection operator $P_{\mathcal{D}}$, followed by a subsequent mapping to the constraint set $\mathcal{E}$ using the projection map $P_{\mathcal{E}}$. The iteration is repeated until $P_{\mathcal{D}}z_{j+1} = P_{\mathcal{D}}z_j$, i.e., until the data association to points in the material data set remains invariant. The convergence properties of the fixed-point solver (13) have been investigated in [16].

Patient-specific models

In this subsection, we first provide the histograms of the complex moduli in the material data sets, binned by voxel, for all eight patients, which are utilized to develop patient-specific models and solve transcranial ultrasound stimulation problem with recourse to our Data-Driven approach. Subsequently, we depict the computed contours of real and imaginary components of both maximum and minimum principal strain across the entire brain for all eight patients.

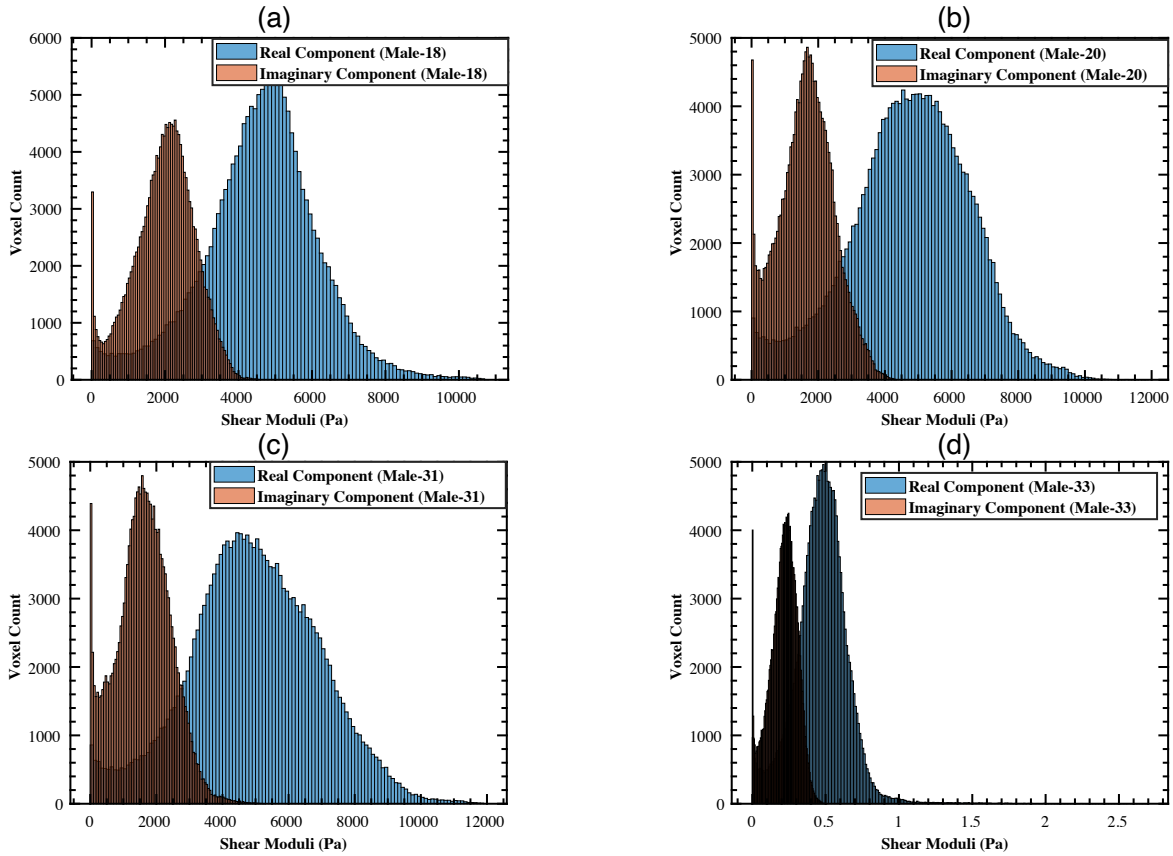

Fig. S1. Data-Driven (DD) brain mechanics allows for patient specific modeling: Histograms of complex shear moduli obtained from MRE data for four different male subjects used for corresponding DD models. Both the geometry and viscoelastic map are obtained from the publicly available MRE data provided by [8].

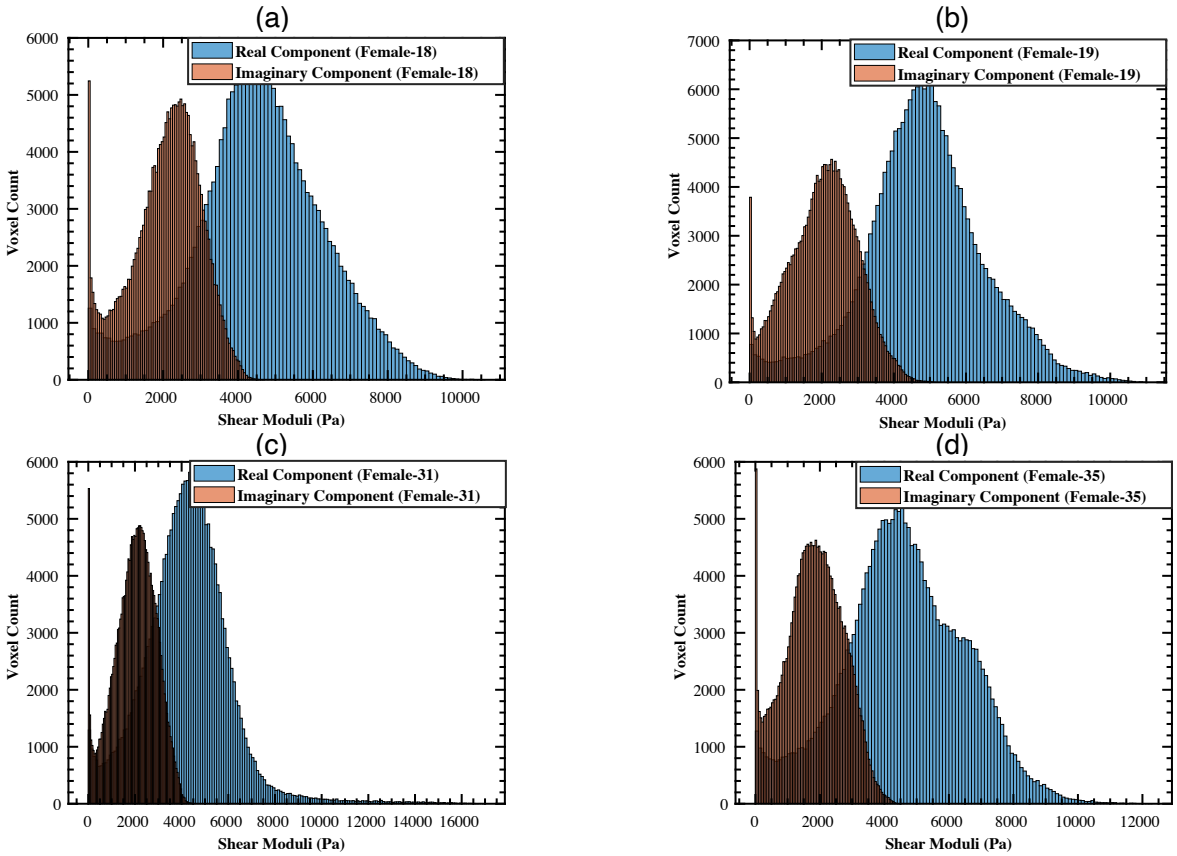

Fig. S2. Data-Driven (DD) brain mechanics allows for patient specific modeling: Histograms of complex shear moduli obtained from MRE data for four different female subjects used for corresponding DD models. Both the geometry and viscoelastic map are obtained from the publicly available MRE data provided by [8].

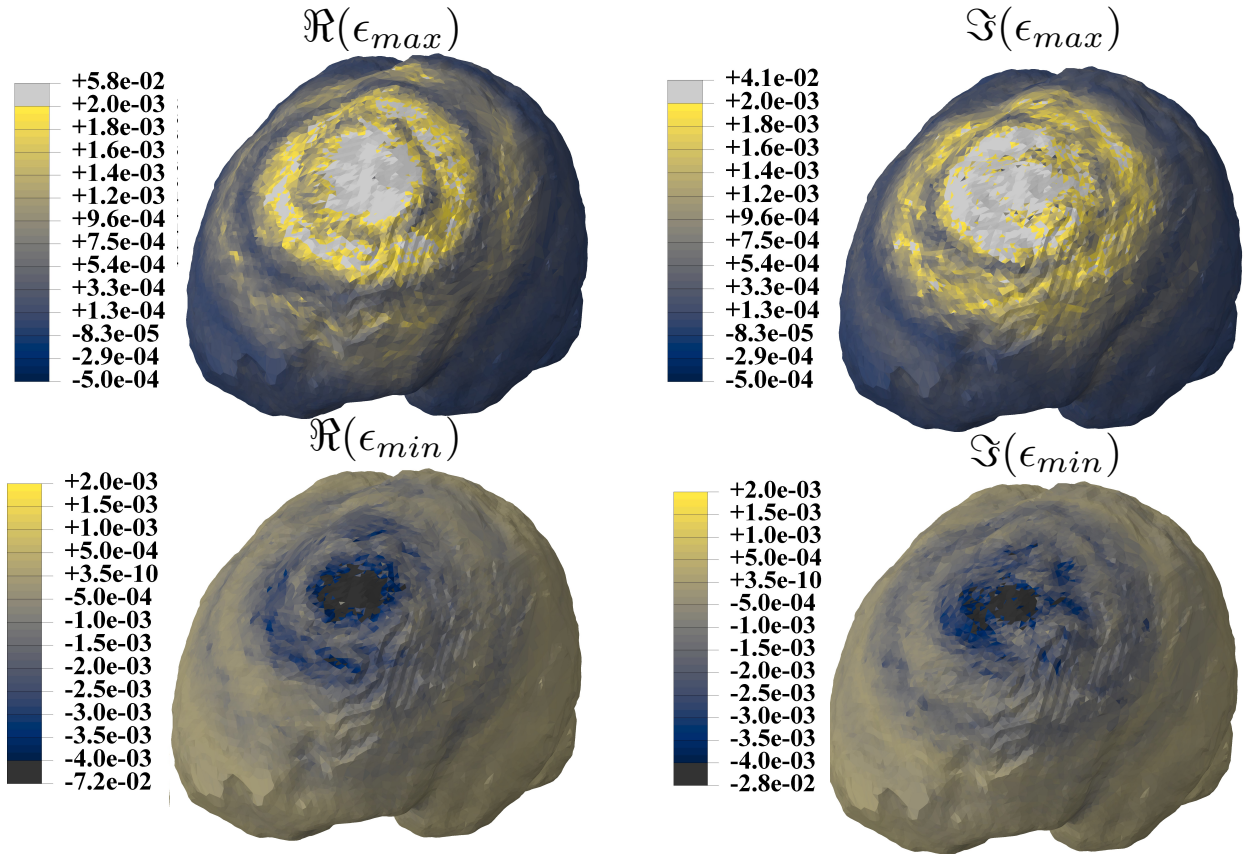

Fig. S3. Patient-specific model for 18 year old male subject: the real and imaginary components of maximum and minimum harmonic principal strain at 50 Hz, accumulated due to application of transcranial ultrasound on a region on the frontal lobe of brain.

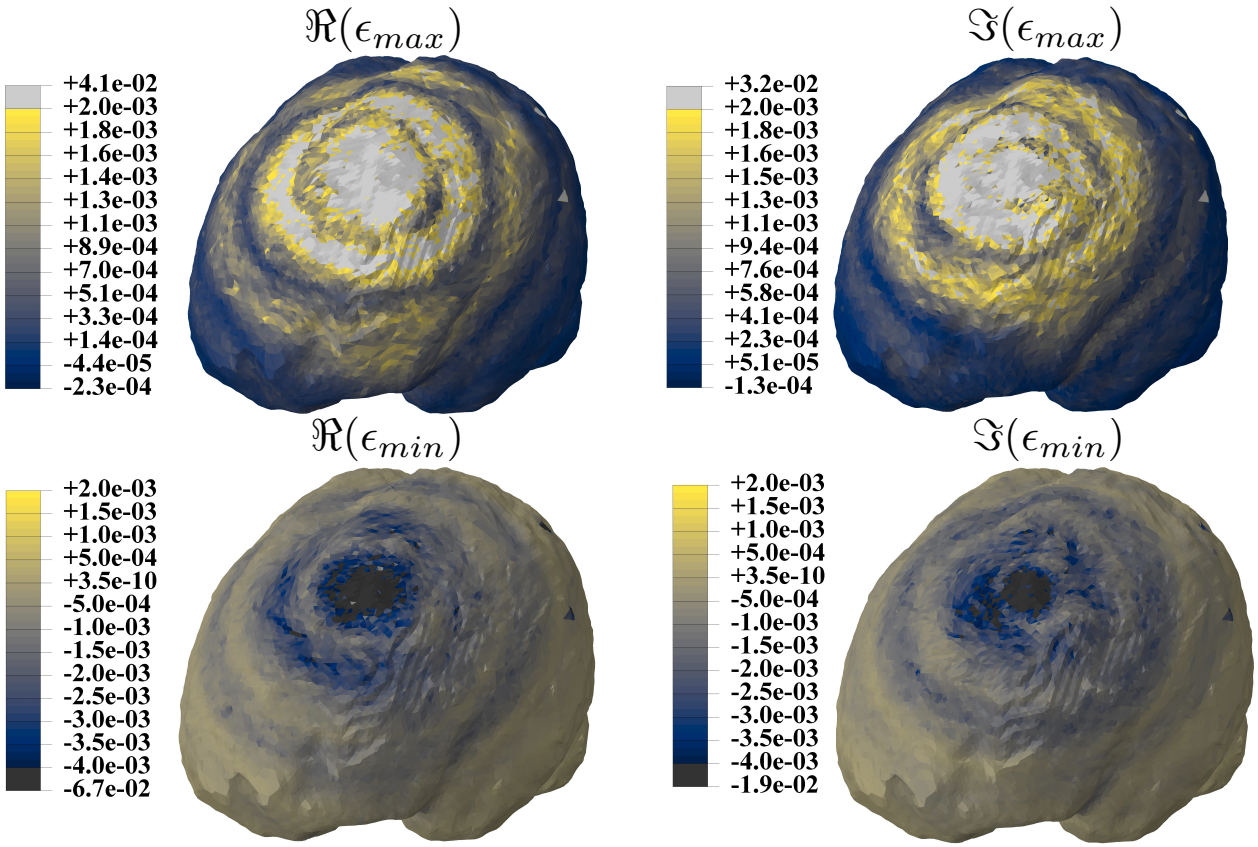

Fig. S4. Patient-specific model for a 20 year old male subject: the real and imaginary components of maximum and minimum harmonic principal strain at 50 Hz, accumulated due to application of transcranial ultrasound on a region on the frontal lobe of brain.

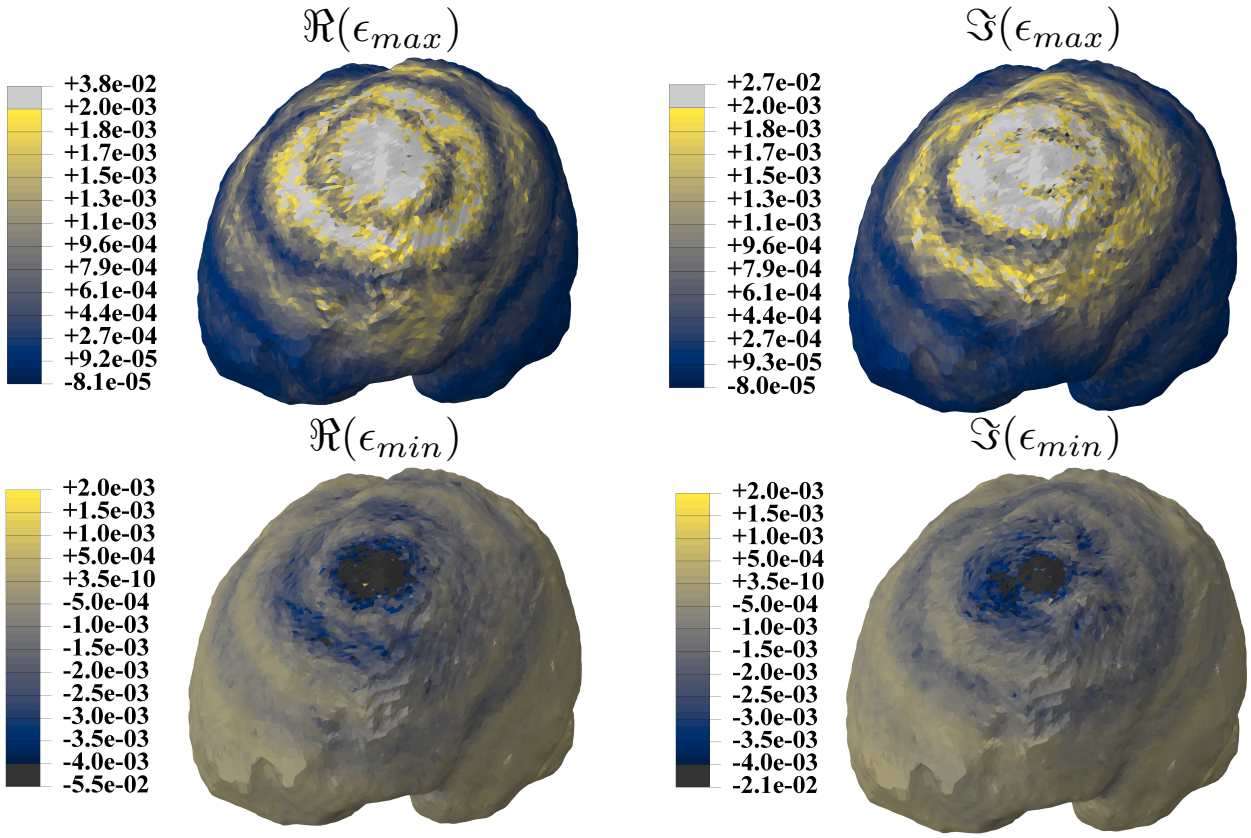

Fig. S5. Patient-specific model for a 31 year old male subject: the real and imaginary components of maximum and minimum harmonic principal strain at 50 Hz, accumulated due to application of transcranial ultrasound on a region on the frontal lobe of brain.

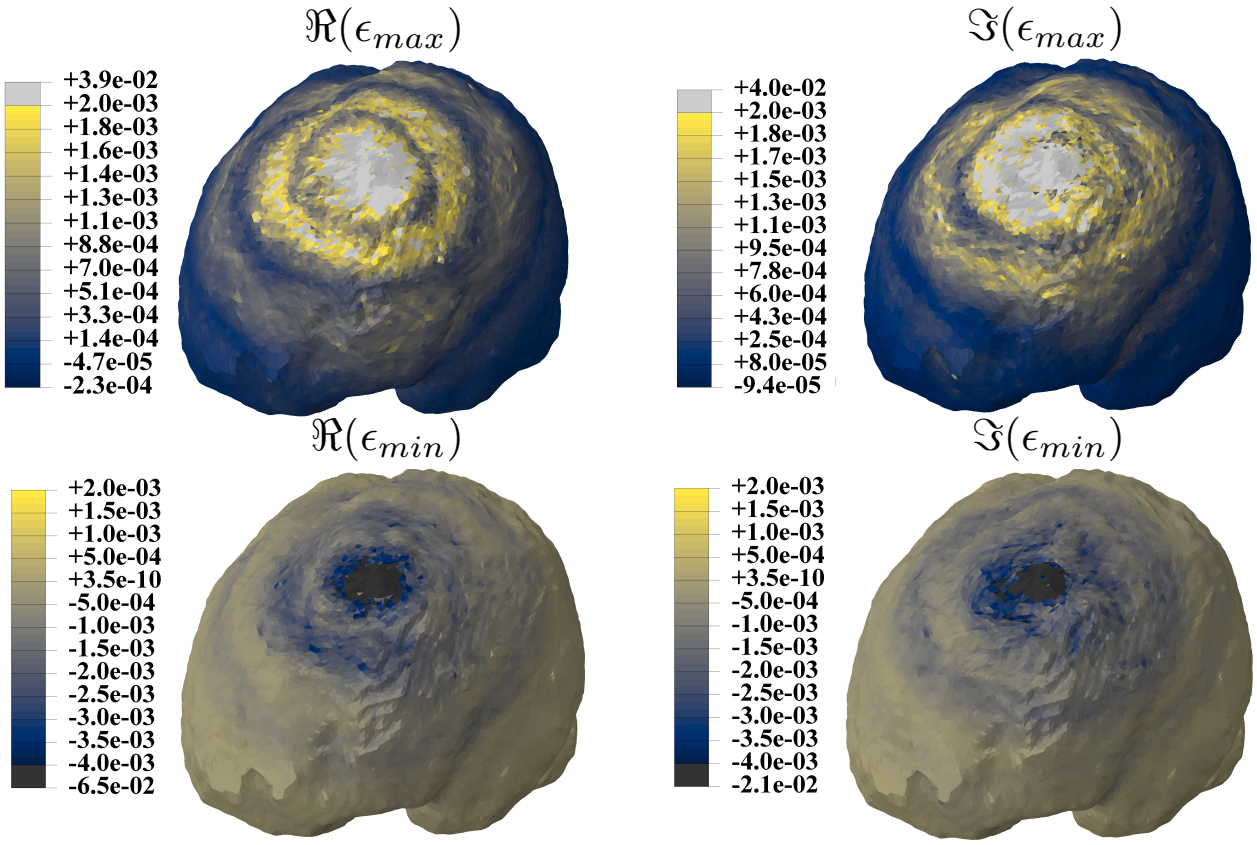

Fig. S6. Patient-specific model for a 33 year old male subject: the real and imaginary components of maximum and minimum harmonic principal strain at 50 Hz, accumulated due to application of transcranial ultrasound on a region on the frontal lobe of brain.

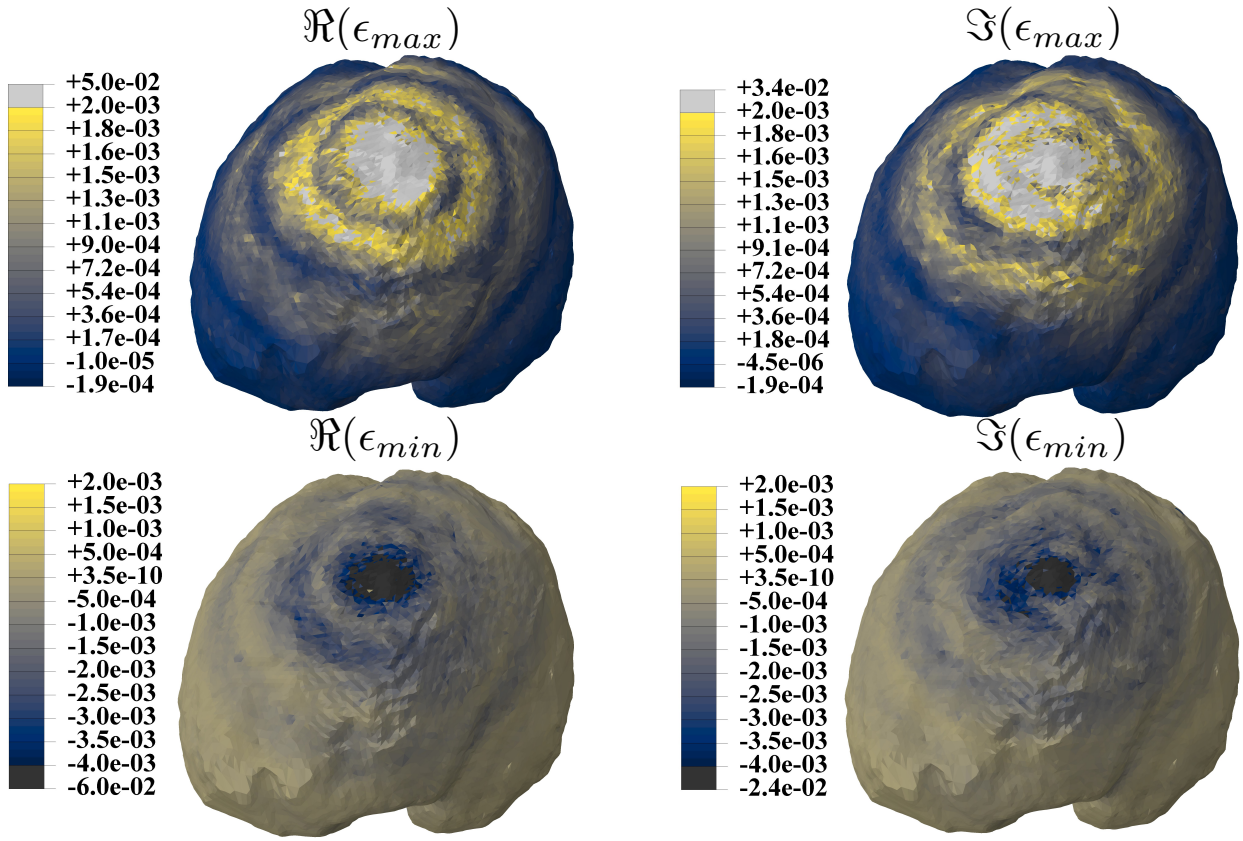

Fig. S7. Patient-specific model for a 19 year old female subject: the real and imaginary components of maximum and minimum harmonic principal strain at 50 Hz, accumulated due to application of transcranial ultrasound on a region on the frontal lobe of brain.

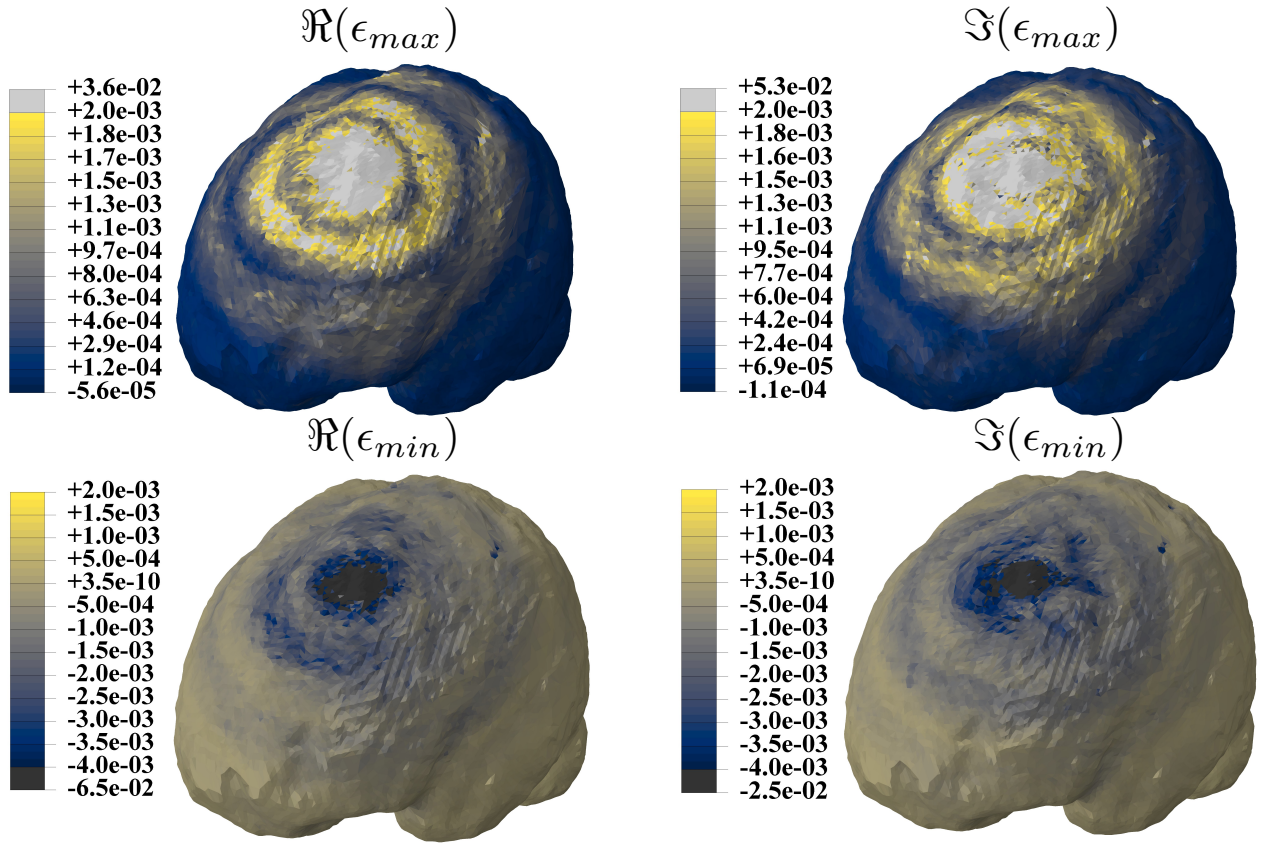

Fig. S8. Patient-specific model for a 18 year old female subject: the real and imaginary components of maximum and minimum harmonic principal strain at 50 Hz, accumulated due to application of transcranial ultrasound on a region on the frontal lobe of brain.

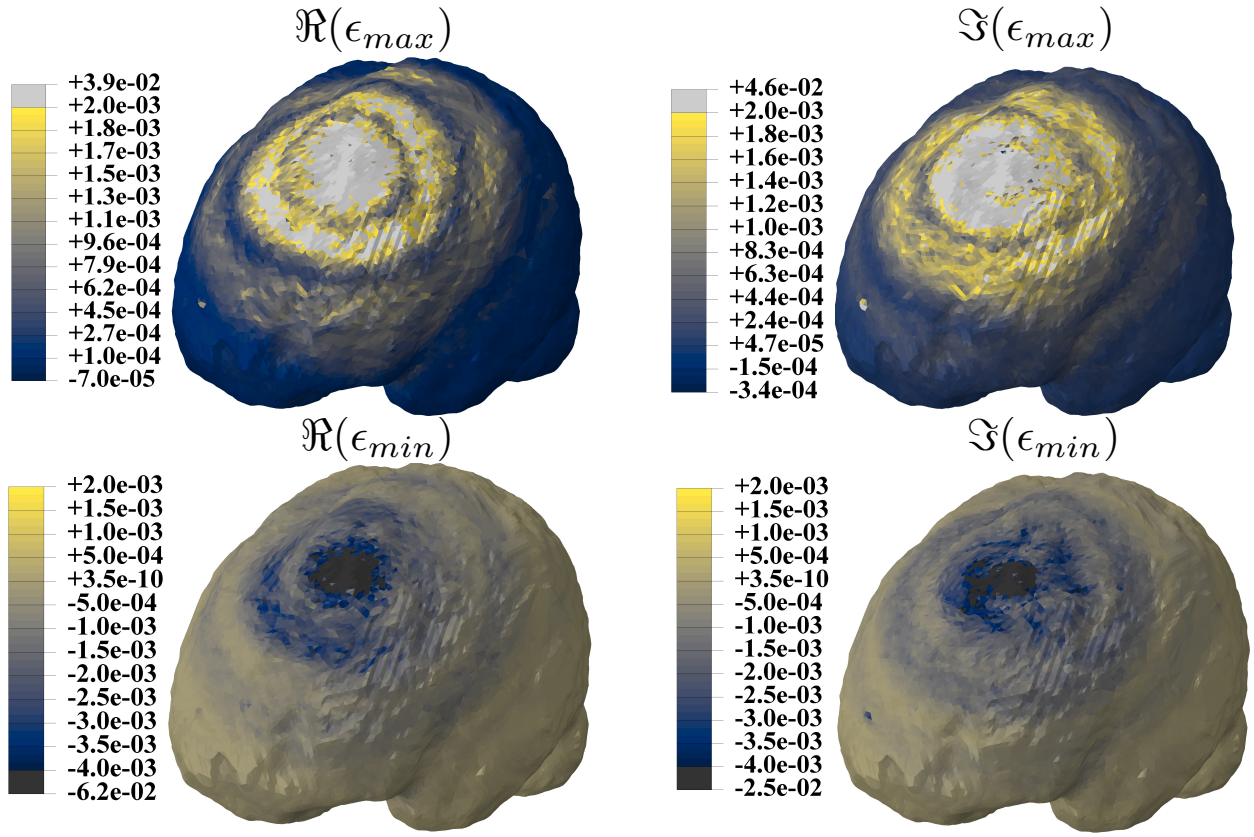

Fig. S9. Patient-specific model for a 31 year old female subject: the real and imaginary components of maximum and minimum harmonic principal strain at 50 Hz, accumulated due to application of transcranial ultrasound on a region on the frontal lobe of brain.

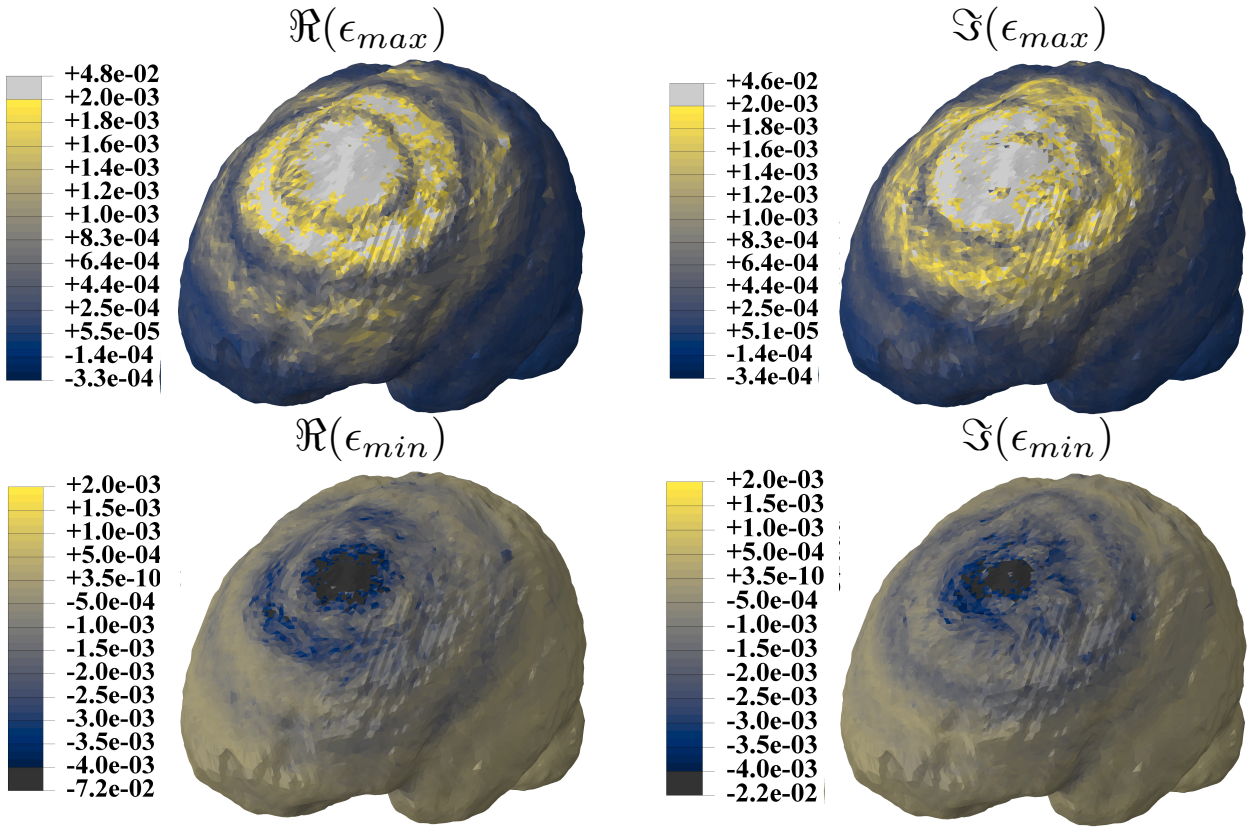

Fig. S10. Patient-specific model for a 35 year old female subject: the real and imaginary components of maximum and minimum harmonic principal strain at 50 Hz, accumulated due to application of transcranial ultrasound on a region on the frontal lobe of brain.